Article

Not peer-reviewed version

Plant Nitrogen Estimation by Developing an Accurate Correlation Between VNIR-Only Vegetation Indexes and Normalized Difference Nitrogen Index

Yücel Çimtay *

Posted Date: 20 July 2023

doi: 10.20944/preprints202307.1328.v1

Keywords: agriculture; land cover; remote sensing; fertilizer; yield

Article

Plant Nitrogen Estimation by Developing an Accurate Correlation between VNIR-Only Vegetation Indexes and Normalized Difference Nitrogen Index

Yücel Çimtay [1]

[1] Computer Engineering, TED University; yucel.cimtay@tedu.edu.tr

Abstract: Nitrogen is crucial for plant physiology due to the fact that plants consume a significant amount of nitrogen during the development period. Nitrogen supports the root, leaf, stem, branch, shoot and fruit development of plants. At the same time, it also increases flowering. To monitor the vegetation nitrogen concentration, one of the best indicator developed in the literature is Normalized Difference Nitrogen Index (NDNI) which is based on the usage of the spectral bands: 1510 and 1680 nm. from Short-Wave Infrared (SWIR) region of electromagnetic spectrum. However, majority of the remote sensing sensors like cameras and/or satellites do not have a SWIR sensor due to the high costs. Many vegetation indexes like NDVI, EVI, MNLI, have been developed in also VNIR region to monitor the greenness and healthy of the crops. However these indexes are not very correlated to the nitrogen content. Therefore, in this study, a novel method is developed which transforms the estimated VNIR band indexes to NDNI by using a regression method between a group of VNIR indexes and NDNI. Training is employed by using VNIR band indexes as input and NDNI as output which are both calculated from the same location. After training, an overall correlation of 0.93 is achieved. Therefore, by using only VNIR band sensors, it is possible to estimate the nitrogen content of the plant with high accuracy.

Keywords: agriculture; land cover; remote sensing; fertilizer; yield

1. Introduction

Numerous physiological activities in leaves, including photosynthesis, respiration, and transpiration, are primarily regulated by nitrogen [1–3]. Nitrogen is also closely related to chlorophyll concentration, light utilization efficiency, and net crop production [4–6]. Besides being a frequently limiting factor for plant growth [7–9], nitrogen is a crucial input in the cycle of ecological processes [10,11]. Leaf nitrogen content has also been suggested as one of the crucial bio-diversity variables for monitoring of the progress towards the Aichi Biodiversity Targets by the remote sensing and ecology communities, who acknowledge the significant role of leaf nitrogen in biodiversity and ecosystem functioning [12,13].

Despite being a relatively minor element of leaves (up to 6.5-7%), nitrogen has been reliably recovered using leaf and canopy-level hyperspectral data [14,15]. By offering contiguous, narrow spectral band data, hyperspectral data are able to identify the nitrogen's small absorption properties. Compared to the conventional destructive sample procedures, this provides an effective and economical way to assess leaf nitrogen. The spectra from leaf powder, dry leaves, and fresh leaves were employed in previous research on the determination of nitrogen concentration in vegetation, as well as estimates at the canopy level [16–18]. The mask of the significant water absorption [17,19], the confounding effects coming from canopy structure, illumination/viewing geometry, and background [20,21], and other obstacles make it difficult to retrieve nitrogen at the canopy level.

To improve the nitrogen content estimation performance, numerous methods have been employed. One method is spectral transformation, which includes employing first/second derivatives and reflectance log transformation [22,23]. There are also other studies which includes continuum removal [17,24], water removal [25,26], and wavelet analysis [27]. Numerous studies have been proposed to estimate the nitrogen content over forests [18,23,28–30], grasslands [31–33], and

 doi:10.20944/preprints202307.1328.v1

crop ecosystems [34–36]. A variety of artificial intelligence techniques, including support vector regression, neural networks, and Bayesian model averaging [32,36,37], as well as traditional regression techniques like stepwise multiple linear regression and partial least square regression, are used to retrieve nitrogen concentration.

Vegetation indices are one of the simplest and most popular empirical methodologies for estimating the biochemical contents of leaves, such as nitrogen. The main sources of nitrogen in leaf cells are proteins and chlorophylls [38]. Since there is a strong correlation between nitrogen and chlorophyll in a variety of species [1,2,39], nitrogen has been estimated using vegetation indices which are proposed and used for chlorophyll estimation [40]. For measuring chlorophyll, spectral wavelengths around 550 nm and 700 nm, as well as the red-edge area (680-780 nm), have been used [35,41], leading to a significant variety of indices [42–44]. In contrast to chlorophyll, there are fewer studies that offer particular indices for nitrogen estimate; the majority of these indices were established for crops [45–48], while just a small number were developed for forests [49].

Given that canopy structure is the primary cause of changes in canopy reflectance, calculation of foliar nitrogen using canopy spectral data is complicated. According to the study in [7], the NIR reflectance (800–850 nm) and canopy foliar mass–based nitrogen concentration (%N) have a significant association that can be utilized to predict nitrogen where in [50] the researchers pointed out that the association between NIR reflectance and canopy structure. The study in [51] suggested that the biological associations between nitrogen and structural characteristics that affect NIR scattering and reflectance served as the foundation for their ideas. Additionally, in [14] and [52], scientists indicated that the canopy structure and leaf characteristics may co-vary among plant functional types, contradicting the study in [53] who claimed that the %N-NIR correlation is inherently false.

The purpose of the study in [54] was to assess how well 32 vegetation indicators collected from airborne hyperspectral imaging performed when used to calculate canopy foliar nitrogen in a mixed temperate forest. For comparison, the widely used partial least squares regression was carried. These vegetation indicators can be divided into three groups, most of which are connected to the biochemical and structural characteristics of vegetation (e.g., nitrogen, chlorophyll, and leaf area index (LAI)). The nitrogen indicators are selected based on how nitrogen absorption characteristics' physical underpinnings affect canopy reflectance. The biological connections between nitrogen, chlorophyll, and canopy structure were used to justify the inclusion of the structural and chlorophyll indices in this study. Nitrogen (N) losses and the ensuing environmental issues are what define the production of vegetable crops [55–57]. The most frequent environmental issues include nitrous oxide (N2O) emissions, ground and surface water contamination, and eutrophication of surface waters [58,59]. These issues are frequently a result of the extensive use of N fertilizer [60], which typically exceeds the requirement of the crops [57,61,62], which is done to ensure optimal growth and production. In order to decrease N contamination of water bodies by intensive vegetable production, it is necessary to understand crop nitrogen requirements and match crop demand with nitrogen supply [57,63,64].

There are numerous techniques available for tracking crop nitrogen status [57,65]. Leaf nutritional analysis is a common method, but it is time-consuming and labor-intensive in the lab, and it typically cannot quantify the temporal and geographical variability of nitrogen status [66,67]. These are significant drawbacks since it is much easier to match the supply of nitrogen to crop requirements when one is aware of the temporal and spatial variability of crop nitrogen status [68].

Optical sensors are tools that quickly, accurately, and nondestructively monitor the crop's nitrogen status in the field [57,69]. They make it possible to regularly evaluate a crop and evaluate spatial variability. Canopy reflectance sensors, which are among the proximal optical sensors, have two highly advantageous characteristics in that they can monitor huge portions of a crop while they are in motion [70]. Field crops' nitrogen status can be evaluated via measures of crop reflectance [65]. These measures are based on the differential reflection of light wavelengths [57], which, depending on crop nitrogen status [69], are absorbed and reflected by the crop in varying amounts. Typically, red, green, and near-infrared light wave lengths are employed for nitrogen estimation [65]. Recently, the red-edge has been suggested as a solution for nitrogen estimation to the red band's apparent saturation [71,72].

The nitrogen nutrition index (NNI) [67,73], is another commonly utilized strategy. The critical crop nitrogen content [74,75] is the lowest crop nitrogen content required for non-limiting growth, and it is used to calculate NNI by dividing the actual crop nitrogen content by it. Any variation from 1 indicates either excess nitrogen (i.e., NNI>1) or insufficient nitrogen (i.e., NNI1) crop status, with values of NNI equal to 1 indicating adequate nitrogen feeding [76].

Due to the high cost of SWIR band sensors, a regression based method should be developed which maps the VNIR band indexes to SWIR band indexes which has more capability to measure the crop nitrogen status like [113]. The majority of studies have been done on cereal crops like wheat [12,79] and rice [80,81]; very few have been done on vegetable crops like sweet pepper.

In [83], the crop nitrogen status of sweet pepper was estimated using eight vegetation indices that were computed from canopy reflectance data taken with two separate proximate sensors. First, crop NNI calibration regression models were fitted for each vegetation index. Second, a different dataset was used to validate these regression equations. Thirdly, sufficient values for each vegetative index for optimal nitrogen nutrition, for the main phenological stages of sweet pepper crops, were obtained utilizing the validated equations between vegetation indices and crop NNI.

The findings of the study [84] supported the use of the normalized difference vegetation index (NDVI) as a useful tool for determining the nitrogen status of cotton leaves at various growth stages. Using vegetation indices, the study in [85] calculated the nitrogen nutrition index (NNI), canopy nitrogen density (CND), and leaf nitrogen content of winter wheat over the course of the entire growth period. This study demonstrated that the correlations between each nitrogen index and the Vogelmann red-edge index (VOG), simple ratio pigment index (SRPI), modified red-edge simple ratio index, and red-edge position based on linear interpolation method (REPliner) were not significantly influenced by growth period, and the estimation model R^2 for CND was higher than 81%. The estimation model's accuracy was higher than NNI, however it would become saturated if CND is calculated using just one vegetation index. The red-edge chlorophyll index, CIred-edge was demonstrated by [86] to be responsive to the canopy structure. The correlation between the nitrogen content of cotton leaves and several spectral ratio measures was examined in [87] who also conducted a cluster analysis based on prediction accuracy and overall accuracy.

The ratio of the red-edge position to the near-infrared band was shown to have a pretty high prediction accuracy and overall accuracy. The estimation of the winter wheat spectral index was investigated by [88] in a variety of environments, seasons, varieties, and growth stages. According to their findings, the growth stage had a significant impact on the performance of various vegetation indices and the choice of a sensitive wavelength for plant nitrogen concentration (PNC) estimation. The simple ratio of reflectivity at 370 nm and 400 nm (R_{370}/R_{400}) displayed the most consistent estimation accuracy in an indoor experiment ($R^2 = 0.58$) and field experiment ($R^2 = 0.51$). According to the studies, there are obvious changes in the relevant spectral index for different crops, or for various kinds and ecological zones of the same crop, when employing the spectral index to estimate crop nitrogen [89,90].

Additionally, compared to employing sensitive spectral features alone or vegetation indexes, modeling techniques like deep machine learning can produce greater prediction effects [91]. These techniques can also be used to monitor agricultural nutrients and growth indicators [92–94]. Support vector machine regression (SVR) was shown to be the most effective method for assessing crop nutrient contents in [95] which evaluated artificial neural network and SVR methods. The authors proposed that the creation of models with large sample sizes is appropriate for an artificial neural network. Hyperspectral reflectance of leaves was used in [90] to study the generalized partial least-squares regression (PLSR) model, and this approach was successful in retrieving leaf nitrogen concentration ($r = 0.85$).

The study in [96] is based on data for two types of drip-irrigated cotton at various growth stages from April 2019 to September 2020. The data include canopy nitrogen density (CND) and leaf nitrogen concentration (LNC) values. Pearson's correlation analysis was used to determine which of

Preprints (www.preprints.org) | NOT PEER-REVIEWED | Posted: 20 July 2023 doi:10.20944/preprints202307.1328.v1

the 30 hyperspectral vegetation indexes and the two nitrogen indexes (LNC and CND) that were used in the three modeling techniques of simple multiple linear regression (MLR), PLSR, and support vector regression (SVR) were relatively stable. The models were employed to investigate the possibility of measuring the nitrogen nutrient status of cotton in each growth period based on a multi-vegetation index in order to give theoretical background for the application of remote sensing technology in cotton nutrition monitoring and diagnostics.

Based on the previous studies conducted in the literature to estimate the nitrogen content of the plant, the contributions of this study are,

- Using the radiance values provided by Hyperion data directly without applying any atmospheric correction.
- Developing a proper deep model which transforms VNIR-only vegetation indexes to NDNI with a high correlation.
- Removing the necessity to have high cost special cameras like SWIR to measure the nitrogen content of the crop.
- Enabling the farmers follow the nitrogen content of the crop progressively and decide when to/not to fertilize.

2. Materials and Methods

Image data of Hyperion sensor was used in this study. As a push-broom hyperspectral instrument, Hyperion is housed on the EO-1 satellite which is depicted in Figure 1.

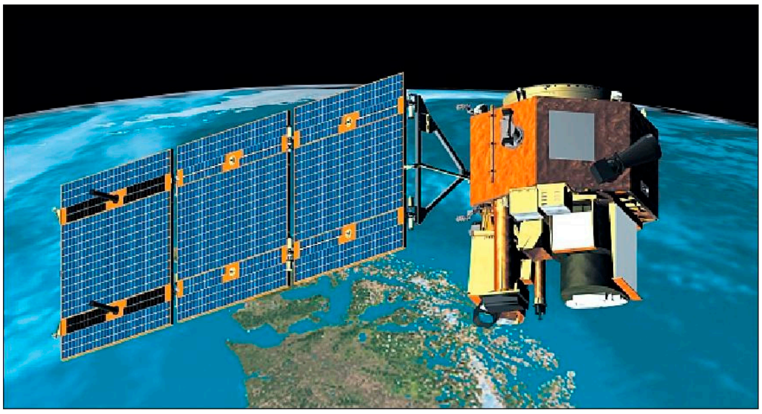

Figure 1. EO-1 Satellite View [97].

With a 10-nm bandwidth spanning from 357 nm to 2576 nm, it collects 220 different spectral channels. All bands have a spatial resolution of (30x30) m^2. The VNIR band, SWIR band, and VNIR-SWIR band indices can all be estimated from the same image data because Hyperion includes both the VNIR and SWIR bands. There is no need for a geometric correction because the Hyperion images have already been rectified geometrically. In addition no atmospheric correction is applied on the data. This is due to the fact that atmospheric correction tools cannot achieve a perfect reconstruction which affects the results negatively. The properties of Hyperion sensor is given in Table 1.

Table 1. Hyperion sensor parameters.

Parameters	Hyperion sensor details
Spectral range	400 – 2500 nm
Spatial resolution	30 m
Radiometric resolution	12 bits
Swath width	7.5 km
Spectral resolution	10 nm
Spectral coverage	Continuous
Number of rows, columns, bands	3271, 871, 220

Preprints (www.preprints.org) | NOT PEER-REVIEWED | Posted: 20 July 2023 doi:10.20944/preprints202307.1328.v1

Different test images were collected from Hyperion data of *Harran* region based in South-West of Turkey. Google Earth and Earth explorer views of *Harran* and Hyperion image are shown in Figure 2.

Harran Plain is a region that starts from the southeast of the city of Şanlıurfa and extends to the Syrian border. It is one of the plains with very fertile soil. It is located between 36°43'-37°08' N parallels and 38°57'-39°55' east meridians in the Upper Mesopotamian lands in Şanlıurfa province.

Mainly corn and cotton farming is done. In the Harran Plain, under the influence of the Mediterranean climate, the continental climate is dominant. Winters are cold and rainy, summers are very hot and dry. Annual precipitation is 365 mm, annual evaporation is 1,848 mm, and annual average temperature is 17.2 °C.

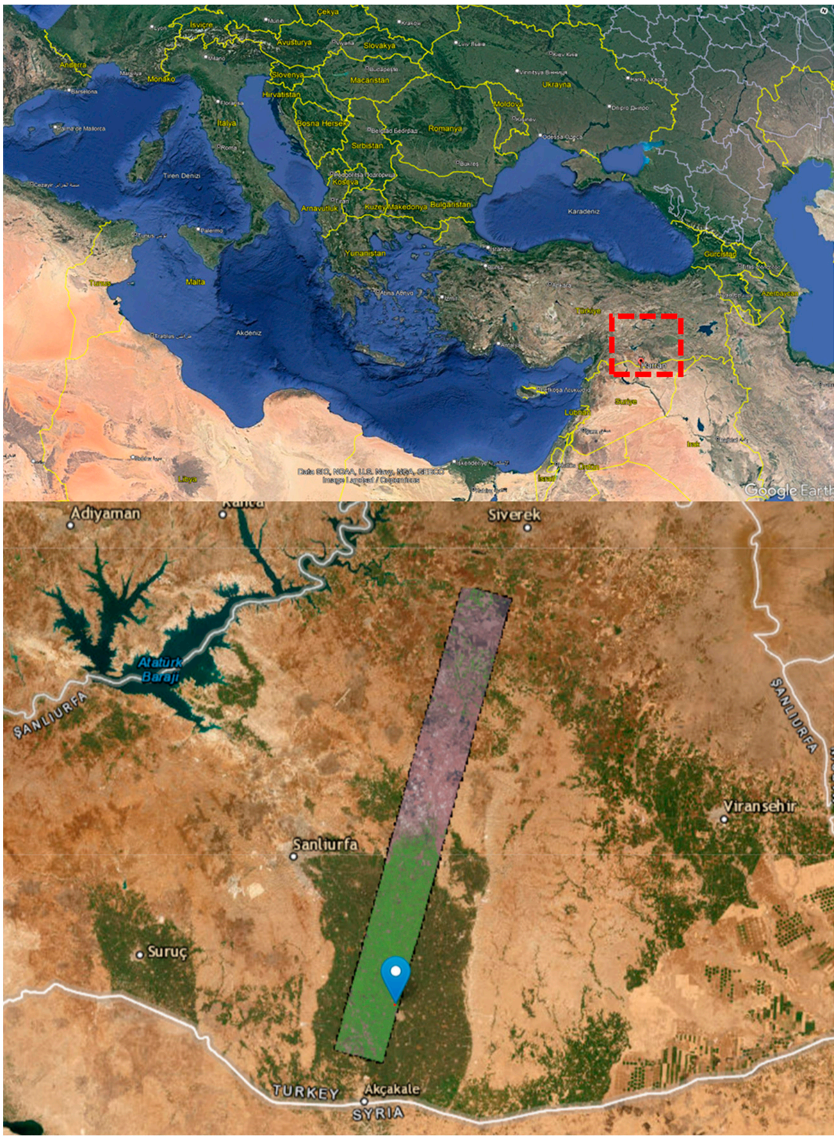

Figure 2. Google-Earth View of Harran (top) and Earth Explorer view of Hyperion color image (bottom).

Hyperion image downloaded from Earth Explorer covers roughly 900 km^2 which is both required and sufficient to investigate the reliability of the proposed method. The QGIS Geographic Information Software Tool is used to determine the area of the Hyperion images [98]. Figure 3 shows the image data taken from *Harran* region in which a large amount of corn, cotton and wheat planting is done by farmers. Image acquisition time is *2016-08-08* when the crop is dense and mature. Image latitude and longitude values and the scale of the map are given on the figure as well.

Preprints (www.preprints.org) | NOT PEER-REVIEWED | Posted: 20 July 2023 doi:10.20944/preprints202307.1328.v1

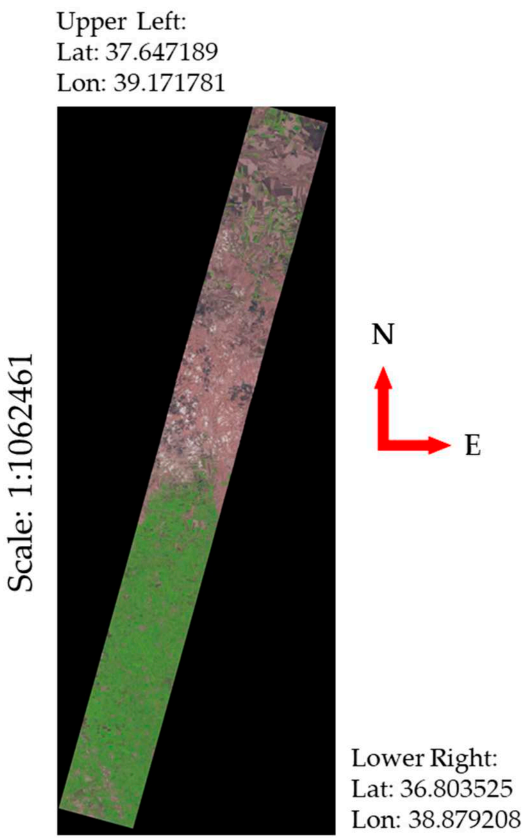

Figure 3. Hyperion Data. RGB Image of Harran Region.

Figure 4 shows a drone camera view and a ground image of a region from Harran taken in July, 2019.

In *Harran* region, to show the vegetation density and the spreading over the area, an NDVI estimation is applied firstly. The Hyperion image and the resulted NDVI index map is shown in Figure 5. Hyperion image has a spatial resolution of 3241x1241, totally 4,022,081 pixels where 2,859,262 pixels are the black regions surrounding the target region. Therefore, vegetation index analysis is implemented on 1,162,819 pixels. Each pixel corresponds to 30x30 m^2 ground area. By recalling that NDVI values can be change from -1 to 1, from the Table 2, it can be seen that the number of pixels have a high NDVI value like > 0.75 is lower, relatively. An important reason for this is the ground spatial resolution of the Hyperion sensor in which one pixel covers 30x30 m^2. This is relatively a large area in which spectral mixing occurs, therefore the spectra of soil, water and vegetation is mixed which may reduce the NDVI indices [100]. Nonetheless the data is powerful and exhibits a good distribution which enables an accurate analysis of vegetation indices.

 doi:10.20944/preprints202307.1328.v1

Figure 4. Harran plain. Drone camera image (top). Ground image from a cotton field (bottom) [99].

Table 2. Number of pixels fall in specific intervals of NDVI values.

NDVI<0	0<=NDVI<0.25	0.25<=NDVI<0.5	0.5<=NDVI<0.75	0.75<=NDVI<1
447,396	193,177	214,010	269,860	49

To increase the accuracy, the pixels with NDVI values higher than 0.2 is taken into account. This is due to typical vegetation pixel has an NDVI greater than 0.2.

The study in [101] states that, NDNI can be used effectively for estimation of the nitrogen content of the vegetation. Since, in this study, we develop a deep model which establish a correlation between VNIR band vegetation indices and NDNI, the most important vegetation indices which hold information about nitrogen content of the plants are estimated. These indices are: NDVI [102], GNDVI [103], EVI [104], GOSAVI [105], GSAVI [105], MCARI2 [106] and VREI2 [107]. To establish the correlation, NDNI [108] is estimated as well. Table 3 shows the corresponding indices, the bands or wavelengths and the equations which are used to estimate them.

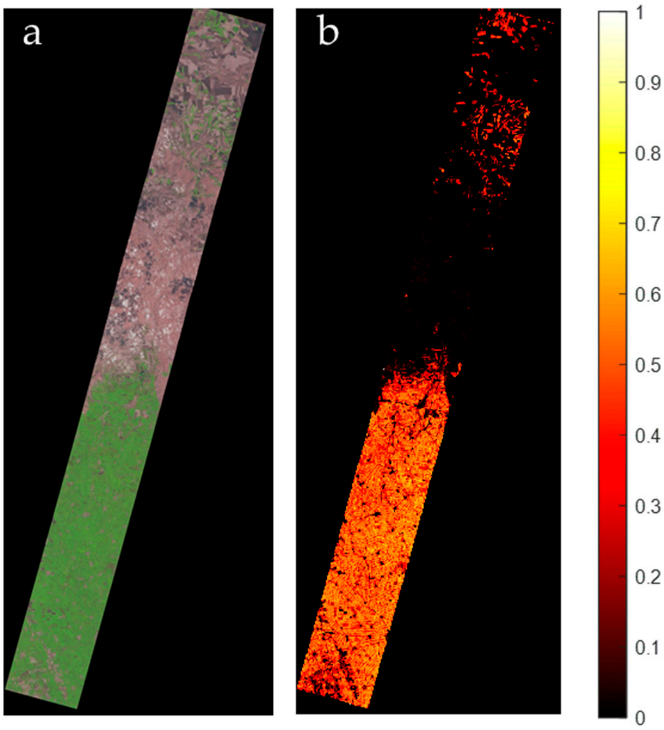

Figure 5. Hyperion image and NDVI Map for *Harran*. a. Hyperion color image b. NDVI Map.

Table 3. Vegetation indices, bands or wavelengths and equations.

Index	Bands and/or Wavelengths	Equation for Estimation
NDVI [102]	NIR, RED	$\frac{NIR - Red}{NIR + Red}$
GNDVI [103]	NIR, Green	$\frac{NIR - Green}{NIR + Green}$
EVI [104]	NIR, Green, Blue	$2.5 * \frac{NIR - Red}{NIR + 6 * Red - 7.5 * Blue + 1}$
GOSAVI [105]	NIR, Green	$\frac{NIR - Green}{NIR + Green + 0.16}$
GSAVI [105]	NIR, Green	$1.5 * \frac{NIR - Green}{NIR + Green + 0.5}$
MCARI2 [106]	$\rho_{800}, \rho_{670}, \rho_{550}$	$\frac{1.5 * [2.5(\rho_{800} - \rho_{670}) - 1.3(\rho_{800} - \rho_{670})]}{\sqrt{(2 * \rho_{800} + 1)^2 - (6 * \rho_{800} - 5 * \sqrt{\rho_{670}}) - 0.5}}$
VREI2 [107]	$\rho_{734}, \rho_{747}, \rho_{726}, \rho_{715}$	$\frac{\rho_{734} - \rho_{747}}{\rho_{715} + \rho_{726}}$
NDNI [108]	ρ_{1510}, ρ_{1680}	$\frac{\log\left(\frac{1}{\rho_{1510}}\right) - \log\left(\frac{1}{\rho_{1680}}\right)}{\log\left(\frac{1}{\rho_{1510}}\right) + \log\left(\frac{1}{\rho_{1680}}\right)}$

The black regions on Hyperion data is excluded first. Then, each vegetation indices are estimated for the pixels left. N to be number of pixels in each index map, a vector of index values is created as shown in equation 1, where Map_{vi} is the index map of the corresponding vegetation index and $index_i$ is the estimated index value at pixel i.

$$Map_{vi} = [index_1, index_2 \ldots index_N] \tag{1}$$

Then, a new index data is created as shown in equation 2, where $I_{v.i.ab}$ is the estimated index for (b). pixel of vegetation index (a). (i.e. 3rd pixel of NDVI map.)

Preprints (www.preprints.org) | NOT PEER-REVIEWED | Posted: 20 July 2023 doi:10.20944/preprints202307.1328.v1

$$data = \begin{bmatrix} I_{v.i.11} & \cdots & I_{v.i.1N} \\ \vdots & \ddots & \vdots \\ I_{v.i.M1} & \cdots & I_{v.i.MN} \end{bmatrix} \quad (2)$$

Since this study uses 7 vegetation index from VNIR region, totally 7 Map_{vi} are created at the beginning. Therefore the size of the data matrix is (7x1,162,819). After handling data matrix, a further analysis is done.

- Due to the division by 0, some index values are calculated as infinite and/or NaN. Therefore, those kind of pixels are found and the corresponding column is deleted.
- Another analysis is also done for the pixels having abnormally large vegetation index. Therefore the index values which has an absolute value above 5 are also deleted from the data.
- Finally 1,113,529 pixel values are used and to normalize the effect of the environment at the time of the capturing, each index row in the data is normalized between -1 and 1. To normalize the data the *normalize* function of *Matlab* is used with a 'range' parameter.

Similarly the above operations are also applied on NDNI Map. Finally, the input data has the shape of (7x1113529) and the output data has (1x1113529).

To train a model which matches the input data to the output data, *Matlab deep learning toolbox* [109] is used. By using this tool, a deep neural network is designed with 4 dense (hidden) layers, each with 25 neurons. Figure 6 shows the designed neural network. Number of input neurons is 7 due to the shape of the input data and 1 for output, hence it is the NDNI index value.

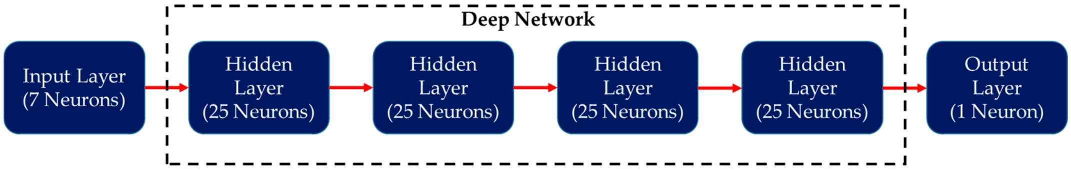

Figure 6. Feed Forward Deep Neural Network (proposed).

Data is split into train, validation and test datasets with the default ratio of 0.7:0.15:0.15. Number of epochs is set as 1000. Training function and adaption learning functions are set as TRAINLM (Levenberg-Marquardt) and LEARNGDM. LEARNGDM is a gradient descent algorithm with momentum. The cost will be pushed farther to go around a saddle point by adding a momentum element to the gradient descent, even though the current gradient is insignificant. Performance function is MSE. Training is done on CPU on a Windows PC with 8 GB Ram and 11th Gen Intel(R) Core(TM) i7-1165G7 @ 2.80GHz processor. The reason not to use GPU is that in *Matlab*, TRAINLM function is not supported.

The Levenberg-Marquardt [110] technique, which was developed for minimizing functions that are sums of squares of nonlinear functions, is derived from Newton's method [111]. Levenberg-Marquardt algorithm is designed to minimize sum-of-square error functions of the form (3). In (3), err_k is the error in the kth instance and err is a vector with element at k. A Taylor series can be used to expand the error vector to first order if the difference between the old and new weight vectors is modest.

$$E = \frac{1}{2}\sum k(err_k)^2 = \frac{1}{2}\|err\|^2 \quad (3)$$

$$err(j+i) = err_j + \frac{\partial err_k}{\partial w_i}(w(j+1) - w(j)) \quad (4)$$

As a result, the error function can be expressed as

$$E = \frac{1}{2}\left\|err(j) + \frac{\partial err_k}{\partial w_i}(w(j+1) - w(j))\right\|^2 \quad (5)$$

After minimizing the error function with respect to the updated weight vector, (6) can be written.

$$w(j+1) = w(j) - (Z^T Z)^{-1} Z^T err(j) \tag{6}$$

where,

$$Z_{ki} \equiv \frac{\partial err_k}{\partial w_i} \tag{7}$$

Since the Hessian for the sum-of-square error function is as shown in (8),

$$H_{ij} = \frac{\partial^2 E}{\partial_{w_i} \partial_{w_j}} + \sum \{(\frac{\partial err_k}{\partial w_i}) \left(\frac{\partial err_k}{\partial w_i}\right) + err_k (\frac{\partial^2 err_k}{\partial w_i \partial w_i})\} \tag{8}$$

By ignoring the second term, Hessian can be written as:

$$H = Z^T Z \tag{9}$$

For nonlinear networks, updating the weights therefore entails the inverse Hessian. Since the Hessian is based on first order derivatives with respect to the network weights, which can be easily handled by back propagation, it can be calculated rather quickly. Although iterative application of the updating formula to reduce the error function is an option, this may provide a step size that is too big, invalidating the linear approximation that the method is based on.

The Levenberg-Marquardt approach minimizes the error function while maintaining a small step size to guarantee the accuracy of the linear approximation. Utilizing a form's customized error function allows for this.

$$E = \frac{1}{2} \left\| err(j) + \frac{\partial err_k}{\partial w_i} (w(j+1) - w(j)) \right\|^2 + \alpha \|(w(j+1) - w(j))\|^2 \tag{10}$$

where α is a parameter adjusting the step size. When the modified error is minimized with respect to $w(j+1)$, (11) is handled.

$$w(j+1) = w(j) - (Z^T Z + \alpha I)^{-1} Z^T e(j) \tag{11}$$

With very large values of α, Levenberg-Marquardt approaches standard gradient descent, whereas for very small values α , approaches to the Newton method.

This study aims to investigate the relation between VNIR-only vegetation indexes and NDNI. For that purpose linear regression is employed by using a deep neural network. Linear regression can be explained as follows:

$$Y = a + bX + \varepsilon \tag{12}$$

where

$$a = \frac{(\sum y)(\sum x^2) - (\sum x)(\sum xy)}{n(\sum x^2) - (\sum x)^2} \tag{13}$$

$$b = \frac{n(\sum xy) - (\sum x)(\sum y)}{n(\sum x^2) - (\sum x)^2} \tag{14}$$

In equation 12, Y is the dependent (outcome) variable, a is y-intercept, b is the slope of the regression line, X is the independent variable, and ε is the error term. The calculation of linear regression includes 3 steps:

1. First, the values of formula components a and b are found by using $\sum x$, $\sum y$, $\sum xy$, and $\sum x^2$
2. Then the values derived in the first step are substituted into a and b

Preprints (www.preprints.org) | NOT PEER-REVIEWED | Posted: 20 July 2023 doi:10.20944/preprints202307.1328.v1

3. Finally, a and b values are used with the formula $Y = a + bX + \varepsilon$ to establish the linear relationship between X and Y variables.

Since a deep neural network is used in this study, the calculation is done by neural network tool defined in *Matlab* and linear regression is employed.

3. Results

Regression and loss plots are given in Figures 7 and 8 respectively for training, validation, test and overall data. R^2 values for test and validation data are above 0.91 and 0.93 respectively which is very promising. Similarly MSE loss values are all below 10^{-4}. Best validation loss score is 7.01x10-5, means 70 over 1 million. As it can be observed from figure 7, there are still some outlier values which does not fit the regression line, however number of those kind of points are very low. The best validation score is achieved at epoch 124, therefore the training was stopped at 130. epoch.

The regression equations between input and output handled for training, validation, test and all data is given in Table 4.

Table 4. Regression Equations between output and target.

Data	Equation for Estimation
Training	$Output = 0.87 * Target + 0.0066$
Validation	$Output = 0.89 * Target + 0.0059$
Test	$Output = 0.83 * Target + 0.0089$
All	$Output = 0.87 * Target + 0.0069$

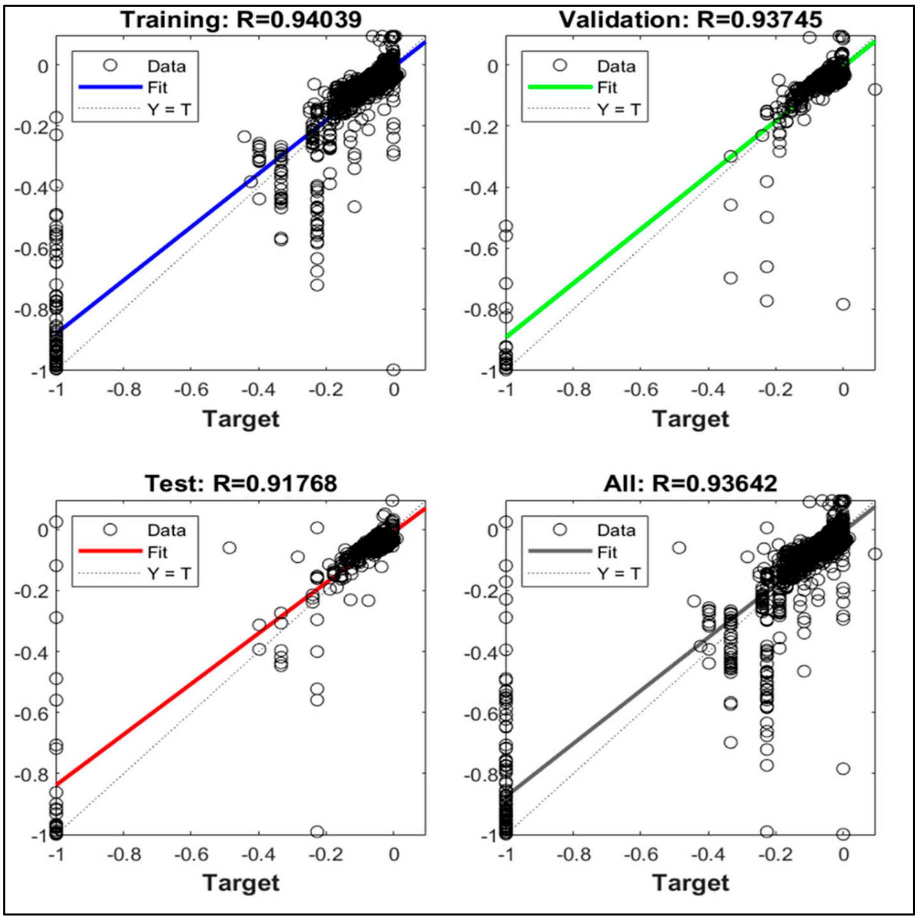

Figure 7. Regression plots for training, validation, test and all data.

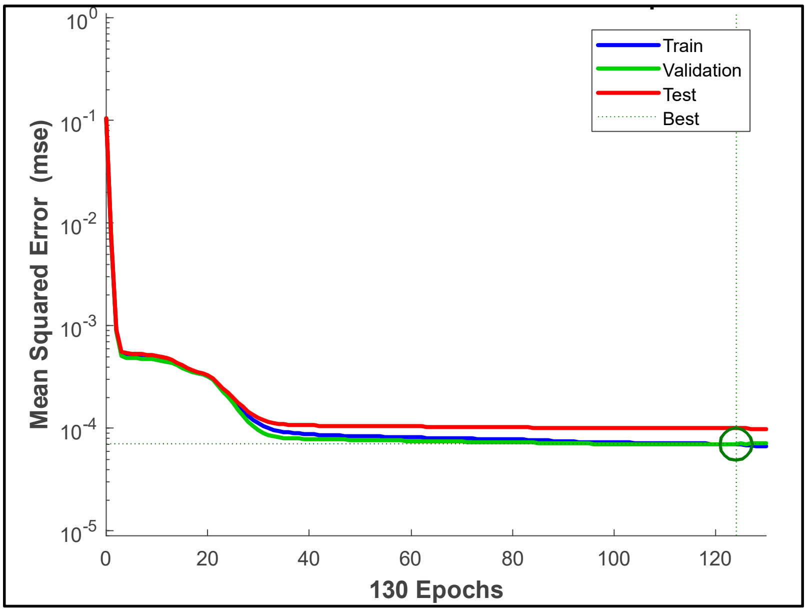

Figure 8. Loss (MSE) for training, validation, test and all data.

3.1. Ablation Study

In this study, a deep neural network is employed to investigate the correlation between VNIR-Only vegetation indexes and NDNI index. For this purpose, various combinations of different networks on normalized and/or unnormalized data is tried. Figure 9 shows the regression results when the depth of the network is reduced to 2 deep layers and data is normalized. Even if test score is improved a bit, validation and all data scores are not good as the proposed network.

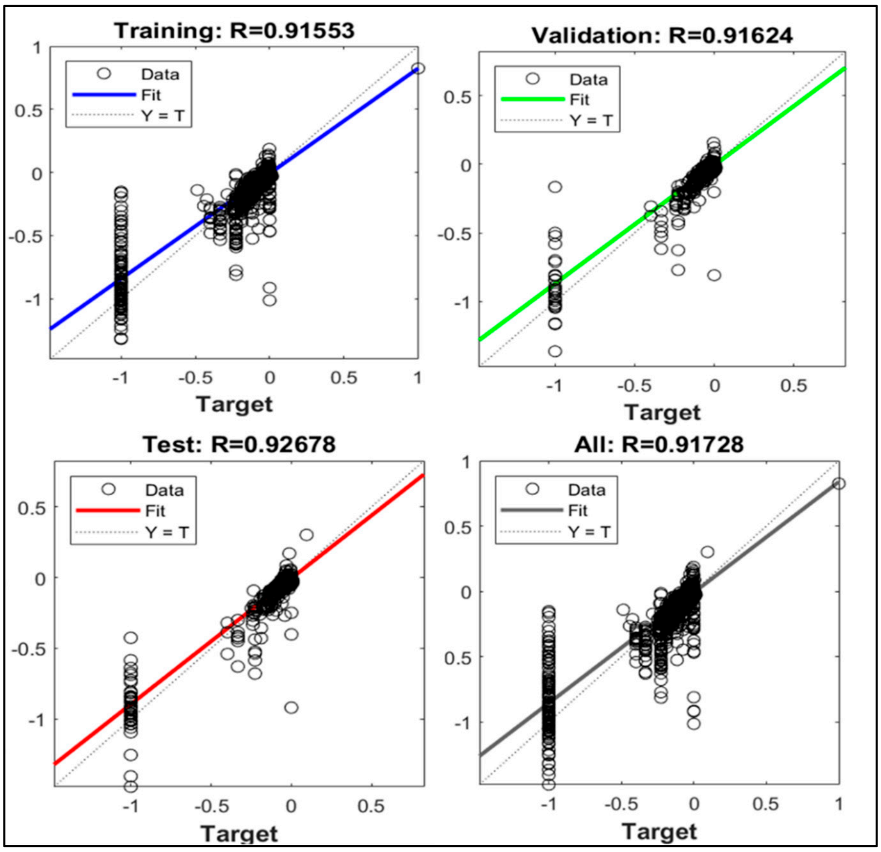

Figure 9. 2 deep layer with 25 neurons on Normalized Data.

Preprints (www.preprints.org) | NOT PEER-REVIEWED | Posted: 20 July 2023 doi:10.20944/preprints202307.1328.v1

Figure 10 shows the regression result for 2 deep layers on unnormalized data which are worse and unbalanced among training, validation and test data. Therefore when the network is not deep enough, normalization of the data is crucial.

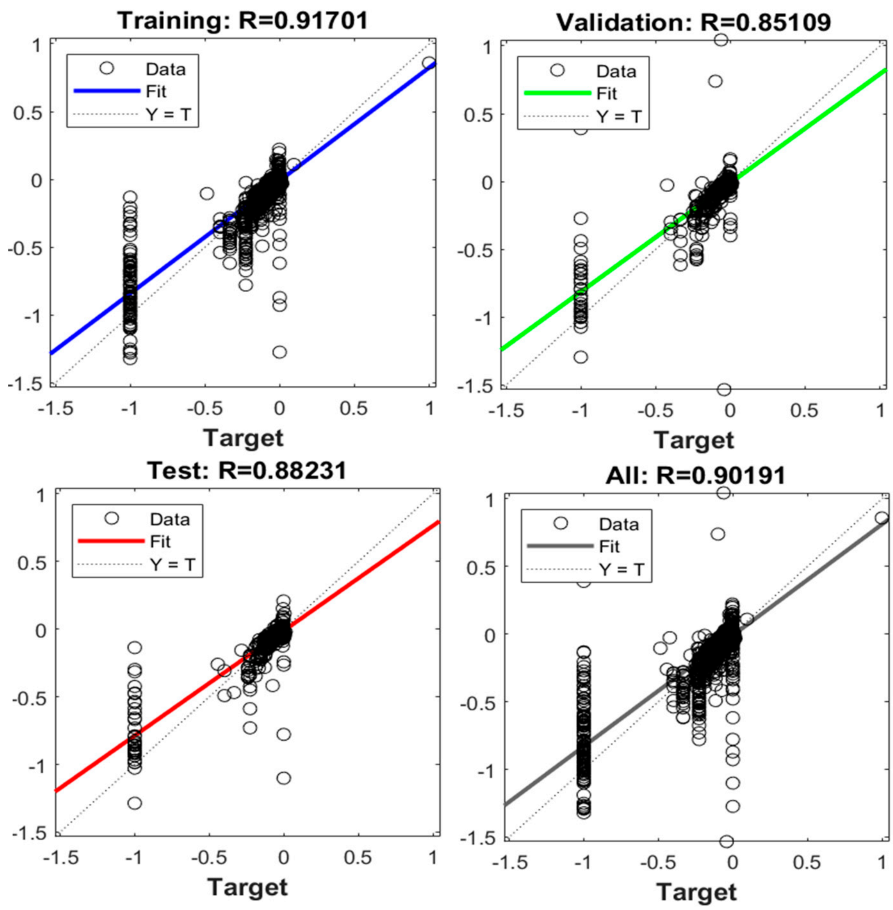

Figure 10. 2 deep layer with 25 neurons on Unnormalized Data.

When the depth of the network is kept and data is not normalized, similar regression results to proposed network can be handled (Figure 11). However still, the results are a bit better when data is normalized. In addition when the data is normalized, the depth of the network can be reduced to two with very little and tolerable reduce of accuracy. By that way, the response time of the network to new data is reduced which is crucial for near real-time and/or real-time applications.

 doi:10.20944/preprints202307.1328.v1

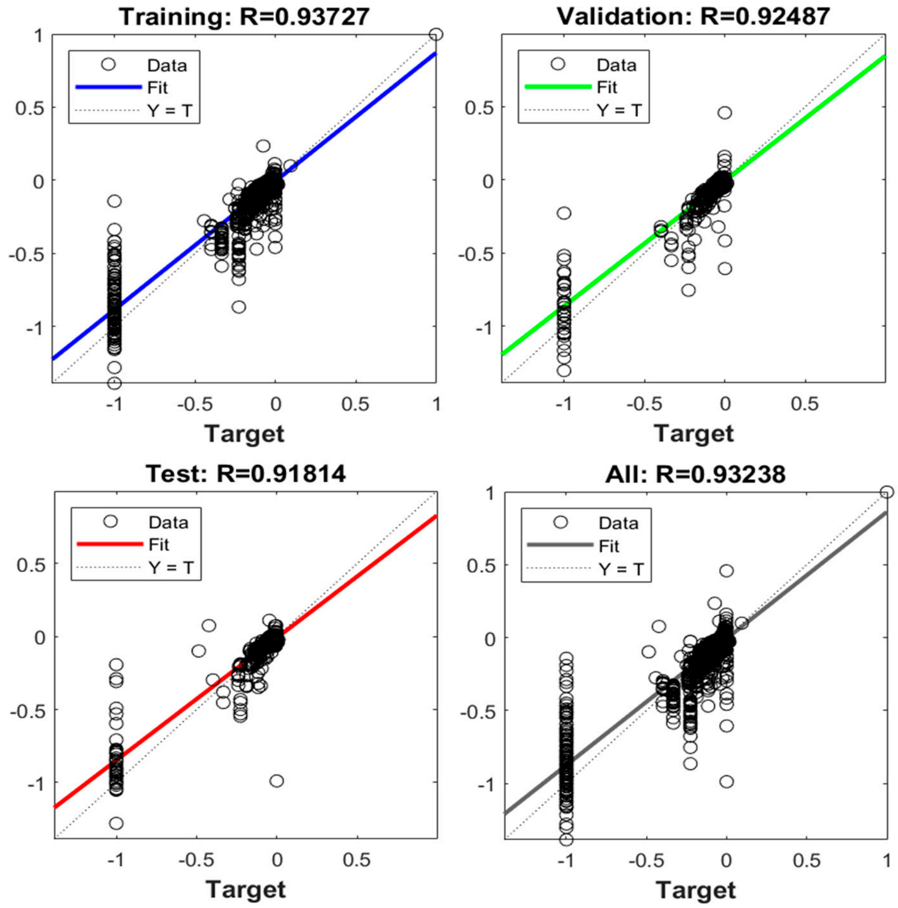

Figure 11. 4 deep layer with 25 neurons on Unnormalized Data.

Various neural networks with different number of deep layers and neurons are trained with the normalized data and the obtained regression scores for train, validation, test and all data are given in Table 5. The best scores are colored in red and the second best score is colored in blue. As (#L, #N) shows the number of deep layers and neurons at each deep layer, (4,15) includes 3 best scores however validation score is low. Similarly (5,15) includes 3 best scores however, test score is low. (3,25) and (4,25) has 3 second best scores and total scores of (4,25) is above (3,25). Other different combinations have 2 best/second best scores, 1 best/second best score or no best/second best scores. Therefore in this study, the combination of (4,25) is proposed.

Table 5. Regression scores obtained by training Various Neural Networks.

Number of Deep Layers	Number of Neurons	Regression scores (Train-Validation-Test-All)
2	10	0.93-0.90-0.85-0.91
3	10	0.93-0.92-0.91-0.92
4	10	0.93-0.91-0.92-0.93
5	10	0.93-0.93-0.90-0.93
2	15	0.92-0.92-0.88-0.91
3	15	0.93-0.91-0.90-0.92
4	15	0.95-0.89-0.93-0.94
5	15	0.94-0.94-0.87-0.93
2	20	0.93-0.92-0.91-0.92
3	20	0.93-0.88-0.91-0.92
4	20	0.95-0.92-0.89-0.94

Preprints (www.preprints.org) | NOT PEER-REVIEWED | Posted: 20 July 2023 doi:10.20944/preprints202307.1328.v1

5	20	0.91-0.92-0.90-0.91
2	25	0.91-0.91-0.92-0.91
3	25	0.94-0.90-0.92-0.93
4	25	0.94-0.93-0.91-0.93
5	25	0.92-0.88-0.89-0.91

After training the network with (4,25), trained model is tested on the Hyperion image. Figure 12 shows the difference image between NDNI and the estimated NDNI with the proposed neural network. It can be observed from the figure that, the difference between estimated and actual NDNI is very low especially for the regions where the vegetation density is high and farming is being done actively.

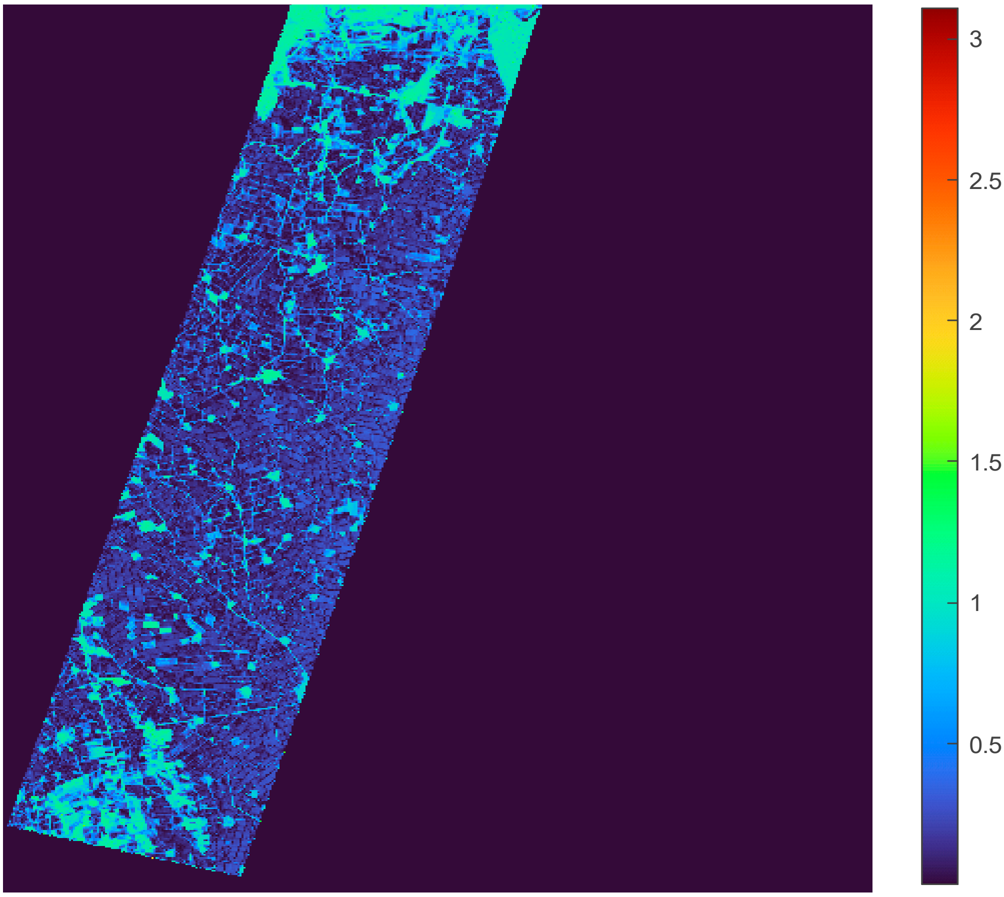

Figure 12. Difference image between actual NDNI and estimated NDNI with proposed Network.

4. Discussion

In this study, the correlation between VNIR-only indexes and NDNI index is investigated and a deep neural network is trained to establish that correlation. The results show that there exists a high correlation between. The most important contribution of this study is proving that the VNIR-Only band vegetation indexes have a high correlation with NDNI which is calculated by using SWIR band region of electromagnetic spectrum. Results show that when VNIR-only indexes are chosen and combined properly and used as the input to a deep neural network, it is possible to establish a high correlation. By this way, the researchers and the farmers do not need to use SWIR band camera which generally means high cost for them. By using VNIR-Only band multispectral/hyperspectral camera and/or satellite, it is possible to estimate the nitrogen content of the plant progressively with a high accuracy. It will enable the farmers to detect the regions with high and/or low amount of nitrogen, so that, they can reduce or increase the fertilization specific to different regions on a field.

Preprints (www.preprints.org) | NOT PEER-REVIEWED | Posted: 20 July 2023 doi:10.20944/preprints202307.1328.v1

To this point, the vegetation index studies in the literature have been based either single electromagnetic region (like VNIR) or multiple regions (VNIR-SWIR). The most important improvement of this study is investigating and establishing the correlation between VNIR-only vegetation indexes and NDNI index. So, without using any SWIR band camera and/or satellite, it can be possible to estimate the nitrogen content easily and with high accuracy and very little loss. The bands used in this study from VNIR region are Red, Green, Blue, NIR, 550nm, 670nm, 715nm, 726nm, 747nm, 734nm and 800nm of Hyperion image data. As it is given in detail in the results section, the correlation (r^2) values are handled above 91% for training, validation, test data by using the proposed deep neural network.

5. Conclusion

In this study, NDNI index which can be calculated by using SWIR bands from electromagnetic spectrum, is estimated by using a proper combination of VNIR band indexes. 7 different vegetation indexes are used as the input and NDNI is used as the output (target) in the training. As a result, very high accuracy is achieved since the correlation for target data is achieved above 91%. Therefore, by using the proposed network, the researchers can estimate the nitrogen content of the plant with respect to NDNI without calculation of NDNI. SWIR band cameras are generally expensive and not easy to be reached. Therefore, the most important contribution of this study is removing the necessity to have a SWIR band camera and atmospheric correction tool to estimate the nitrogen content. In addition, by using the VNIR-only vegetation indexes which are proposed in this study, a specific camera which has the capability of estimating the nitrogen content directly can be produced in the future. It can be used either standalone or integrated on a satellite. When it is used standalone, the real-time tracking of the nitrogen content of the vegetation can be achieved. This study employs a deep neural network to achieve that purpose. In addition, the Hyperion data used in this study and the trained network is shared at https://github.com/ycimtay/VNIR_to_NDNI

Funding: This research received no external funding.

Yücel CIMTAY graduated from Bilkent University's Electrical & Electronics Engineering department with a bachelor's degree in 2008. In 2018, he finished his PhD at Ankara University. Between 2013 to 2018, he worked as an R&D Engineer for HAVELSAN A.S. Between 2018 and 2020; he worked as a Postdoctoral Research Associate at the Institute for Digital Technologies, Loughborough University London. He is currently an Assistant Professor at TED University. His research areas are, image and signal processing, computer vision and machine learning.

References

1. Field, C.; Mooney, H.A. The photosynthesis-nitrogen relationship in wild plants. In On the Economy of Plant Form and Function; Givnish, T.J., Ed.; Cambridge University Press: Cambridge, UK, 1986; pp. 25–55.
2. Evans, J. Photosynthesis and nitrogen relationships in leaves of C3 plants. Oecologia 1989, 78, 9–19.
3. Reich, P.B.; Ellsworth, D.S.; Walters, M.B. Leaf structure (specific leaf area) modulates photosynthesis–nitrogen relations: Evidence from within and across species and functional groups. Funct. Ecol. 1998, 12, 948–958.
4. Smith, M.L.; Ollinger, S.V.; Martin, M.E.; Aber, J.D.; Hallett, R.A.; Goodale, C.L. Direct estimation of aboveground forest productivity through hyperspectral remote sensing of canopy nitrogen. Ecol. Appl. 2002, 12, 1286–1302.
5. Green, D.S.; Erickson, J.E.; Kruger, E.L. Foliar morphology and canopy nitrogen as predictors of light-use efficiency in terrestrial vegetation. Agric. For. Meteorol. 2003, 115, 163–171.
6. Ollinger, S.V.; Smith, M.L. Net primary production and canopy nitrogen in a temperate forest landscape: An analysis using imaging spectroscopy, modeling and field data. Ecosystems 2005, 8, 760–778.

Preprints (www.preprints.org) | NOT PEER-REVIEWED | Posted: 20 July 2023 doi:10.20944/preprints202307.1328.v1

7. Ollinger, S.V.; Richardson, A.D.; Martin, M.E.; Hollinger, D.Y.; Frolking, S.E.; Reich, P.B.; Plourde, L.C.; Katul, G.G.; Munger, J.W.; Oren, R.; et al. Canopy nitrogen, carbon assimilation, and albedo in temperate and boreal forests: Functional relations and potential climate feedbacks. Proc. Natl. Acad. Sci. USA 2008, 105, 19336–19341.
8. Sievering, H.; Fernandez, I.; Lee, J.; Hom, J.; Rustad, L. Forest canopy uptake of atmospheric nitrogen deposition at eastern US conifer sites: Carbon storage implications? Glob. Biogeochem. Cycles 2000, 14, 1153–1159.
9. Lamarque, J.F.; Kiehl, J.T.; Brasseur, G.P.; Butler, T.; Cameron-Smith, P.; Collins, W.D.; Collins, W.J.; Granier, C.; Hauglustaine, D.; Hess, P.G.; et al. Assessing future nitrogen deposition and carbon cycle feedback using a multimodel approach: Analysis of nitrogen deposition. J. Geophys. Res. Atmos. 2005, 110, 1–21.
10. Plummer, S.E. Perspectives on combining ecological process models and remotely sensed data. Ecol. Model. 2000, 129, 169–186.
11. Zhang, C.; Li, C.; Chen, X.; Luo, G.; Li, L.; Li, X.; Yan, Y.; Shao, H. A spatial-explicit dynamic vegetation model that couples carbon, water, and nitrogen processes for arid and semiarid ecosystems. J. Arid Land 2013, 5, 102–117.
12. Pereira, H.M.; Ferrier, S.; Walters, M.; Geller, G.N.; Jongman, R.H.G.; Scholes, R.J.; Bruford, M.W.; Brummitt, N.; Butchart, S.H.M.; Cardoso, A.C.; et al. Essential biodiversity variables. Science 2013, 339, 277–278.
13. Skidmore, A.K.; Pettorelli, N.; Coops, N.C.; Geller, G.N.; Hansen, M.; Lucas, R.; Mücher, C.A.; O'Connor, B.; Paganini, M.; Pereira, H.M.; et al. Environmental science: Agree on biodiversity metrics to track from space. Nature 2015, 523, 403–405.
14. Wright, I.J.; Reich, P.B.; Westoby, M.; Ackerly, D.D.; Baruch, Z.; Bongers, F.; Cavender-Bares, J.; Chapin, T.; Cornellssen, J.H.C.; Diemer, M.; et al. The worldwide leaf economics spectrum. Nature 2004, 428, 821–827.
15. Kokaly, R.F.; Asner, G.P.; Ollinger, S.V.; Martin, M.E.; Wessman, C.A. Characterizing canopy biochemistry from imaging spectroscopy and its application to ecosystem studies. Remote Sens. Environ. 2009, 113, S78–S91.
16. Curran, P.J. Remote sensing of foliar chemistry. Remote Sens. Environ. 1989, 30, 271–278. Remote Sens. 2016, 8, 491 16 of 20
17. Kokaly, R.F.; Clark, R.N. Spectroscopic determination of leaf biochemistry using band-depth analysis of absorption features and stepwise multiple linear regression. Remote Sens. Environ. 1999, 67, 267–287.
18. Martin, M.E.; Plourde, L.C.; Ollinger, S.V.; Smith, M.L.; McNeil, B.E. A generalizable method for remote sensing of canopy nitrogen across a wide range of forest ecosystems. Remote Sens. Environ. 2008, 112, 3511–3519.
19. Fourty, T.; Baret, F. On spectral estimates of fresh leaf biochemistry. Int. J. Remote Sens. 1998, 19, 1283–1297.
20. Asner, G.P. Biophysical and biochemical sources of variability in canopy reflectance. Remote Sens. Environ. 1998, 64, 234 253.
21. Zarco-Tejada, P.J.; Miller, J.R.; Noland, T.L.; Mohammed, G.H.; Sampson, P.H. Scaling-up and model inversion methods with narrowband optical indices for chlorophyll content estimation in closed forest canopies with hyperspectral data. IEEE Trans. Geosci. Remote Sens. 2001, 39, 1491–1507.
22. Yoder, B.J.; Pettigrew-Crosby, R.E. Predicting nitrogen and chlorophyll content and concentrations from reflectance spectra (400–2500 nm) at leaf and canopy scales. Remote Sens. Environ. 1995, 53, 199–211.
23. Coops, N.C.; Smith, M.L.; Martin, M.E.; Ollinger, S.V. Prediction of eucalypt foliage nitrogen content from satellite-derived hyperspectral data. IEEE Trans. Geosci. Remote Sens. 2003, 41, 1338–1346.
24. Huang, Z.; Turner, B.J.; Dury, S.J.; Wallis, I.R.; Foley, W.J. Estimating foliage nitrogen concentration from HYMAP data using continuum removal analysis. Remote Sens. Environ. 2004, 93, 18–29.
25. Schlerf, M.; Atzberger, C.; Hill, J.; Buddenbaum, H.; Werner, W.; Schueler, G. Retrieval of chlorophyll and nitrogen in Norway spruce (Picea abies L. Karst.) using imaging spectroscopy. Int. J. Appl. Earth Obs. Geoinf. 2010, 12, 17–26.
26. Ramoelo, A.; Skidmore, A.K.; Schlerf, M.; Mathieu, R.; Heitkönig, I.M.A. Water-removed spectra increase the retrieval accuracy when estimating savanna grass nitrogen and phosphorus concentrations. ISPRS J. Photogramm. Remote Sens. 2011, 66, 408–417.

27. Ferwerda, J.G.; Jones, S.D. Continuous wavelet transformations for hyperspectral feature detection. In Progress in Spatial Data Handling; Riedl, A., Kainz, W., Elmes, G.A., Eds.; Springer-Berlin: Heidelberg, Germany, 2006; pp. 167–178.
28. Asner, G.P.; Martin, R.E. Airborne spectranomics: Mapping canopy chemical and taxonomic diversity in tropical forests. Front. Ecol. Environ. 2008, 7, 269–276.
29. Gökkaya, K.; Thomas, V.; Noland, T.L.; McCaughey, H.; Morrison, I.; Treitz, P. Prediction of macronutrients at the canopy level using spaceborne imaging spectroscopy and LiDAR data in a mixedwood boreal forest. Remote Sens. 2015, 7, 9045–9069.
30. Singh, A.; Serbin, S.P.; McNeil, B.E.; Kingdon, C.C.; Townsend, P.A. Imaging spectroscopy algorithms for mapping canopy foliar chemical and morphological traits and their uncertainties. Ecol. Appl. 2015, 25, 2180–2197.
31. Mutanga, O.; Skidmore, A.K.; Prins, H.H.T. Predicting in situ pasture quality in the Kruger National Park, South Africa, using continuum-removed absorption features. Remote Sens. Environ. 2004, 89, 393–408.
32. Skidmore, A.K.; Ferwerda, J.G.; Mutanga, O.; Van Wieren, S.E.; Peel, M.; Grant, R.C.; Prins, H.H.T.; Balcik, F.B.; Venus, V. Forage quality of savannas—Simultaneously mapping foliar protein and polyphenols for trees and grass using hyperspectral imagery. Remote Sens. Environ. 2010, 114, 64–72.
33. Pellissier, P.A.; Ollinger, S.V.; Lepine, L.C.; Palace, M.W.; McDowell, W.H. Remote sensing of foliar nitrogen in cultivated grasslands of human dominated landscapes. Remote Sens. Environ. 2015, 167, 88–97.
34. Inoue, Y.; Sakaiya, E.; Zhu, Y.; Takahashi, W. Diagnostic mapping of canopy nitrogen content in rice based on hyperspectral measurements. Remote Sens. Environ. 2012, 126, 210–221.
35. Li, F.; Miao, Y.; Feng, G.; Yuan, F.; Yue, S.; Gao, X.; Liu, Y.; Liu, B.; Ustin, S.L.; Chen, X. Improving estimation of summer maize nitrogen status with red edge-based spectral vegetation indices. Field Crops Res. 2014, 157, 111–123.
36. Yao, X.; Huang, Y.; Shang, G.; Zhou, C.; Cheng, T.; Tian, Y.; Cao, W.; Zhu, Y. Evaluation of six algorithms to monitor wheat leaf nitrogen concentration. Remote Sens. 2015, 7, 14939–14966. Remote Sens. 2016, 8, 491 17 of 20
37. Axelsson, C.; Skidmore, A.K.; Schlerf, M.; Fauzi, A.; Verhoef, W. Hyperspectral analysis of mangrove foliar chemistry using PLSR and support vector regression. Int. J. Remote Sens. 2013, 34, 1724–1743.
38. Kokaly, R.F.; Asner, G.P.; Ollinger, S.V.; Martin, M.E.; Wessman, C.A. Characterizing canopy biochemistry from imaging spectroscopy and its application to ecosystem studies. Remote Sens. Environ. 2009, 113, S78–S91.
39. Homolova, L.; Maenovsky, Z.; Clevers, J.; Garcia-Santos, G.; Schaeprnan, M.E. Review of optical-based remote sensing for plant trait mapping. Ecol. Complex. 2013, 15, 1–16.
40. Le Maire, G.; Francois, C.; Soudani, K.; Berveiller, D.; Pontailler, J.Y.; Breda, N.; Genet, H.; Davi, H.; Dufrene, E. Calibration and validation of hyperspectral indices for the estimation of broadleaved forest leaf chlorophyll content, leaf mass per area, leaf area index and leaf canopy biomass. Remote Sens. Environ. 2008, 112, 3846–3864.
41. Wu, C.; Niu, Z.; Tang, Q.; Huang, W. Estimating chlorophyll content from hyperspectral vegetation indices: Modeling and validation. Agric. For. Meteorol. 2008, 148, 1230–1241.
42. Main, R.; Cho, M.A.; Mathieu, R.; O'Kennedy, M.M.; Ramoelo, A.; Koch, S. An investigation into robust spectral indices for leaf chlorophyll estimation. ISPRS J. Photogramm. Remote Sens. 2011, 66, 751–761.
43. Sims, D.A.; Gamon, J.A. Relationships between leaf pigment content and spectral reflectance across a wide range of species, leaf structures and developmental stages. Remote Sens. Environ. 2002, 81, 337–354.
44. Le Maire, G.; Francois, C.; Dufrene, E. Towards universal broad leaf chlorophyll indices using PROSPECT simulated da tabase and hyperspectral reflectance measurements. Remote Sens. Environ. 2004, 89, 1–28.
45. Miphokasap, P.; Honda, K.; Vaiphasa, C.; Souris, M.; Nagai, M. Estimating canopy nitrogen concentration in sugarcane using field imaging spectroscopy. Remote Sens. 2012, 4, 1651–1670
46. Tian, Y.C.; Yao, X.; Yang, J.; Cao, W.X.; Hannaway, D.B.; Zhu, Y. Assessing newly developed and published vegetation indices for estimating rice leaf nitrogen concentration with ground- and space-based hyperspectral reflectance. Field Crops Res. 2011, 120, 299–310.
47. Wang, W.; Yao, X.; Yao, X.; Tian, Y.; Liu, X.; Ni, J.; Cao, W.; Zhu, Y. Estimating leaf nitrogen concentration with three-band vegetation indices in rice and wheat. Field Crops Res. 2012, 129, 90–98.

48. Gitelson, A.A.; Vina, A.; Ciganda, V.; Rundquist, D.C.; Arkebauer, T.J. Remote estimation of canopy chlorophyll content in crops. Geophys. Res. Lett. 2005, 32, 1–4.
49. Serrano, L.; Peñuelas, J.; Ustin, S.L. Remote sensing of nitrogen and lignin in Mediterranean vegetation from AVIRIS data: Decomposing biochemical from structural signals. Remote Sens. Environ. 2002, 81, 355–364.
50. Knyazikhin, Y.; Schull, M.A.; Stenberg, P.; Mottus, M.; Rautiainen, M.; Yang, Y.; Marshak, A.; Latorre Carmona, P.; Kaufmann, R.K.; Lewis, P.; et al. Hyperspectral remote sensing of foliar nitrogen content. Proc. Natl. Acad. Sci. USA 2013, 110, E185–E192.
51. Ollinger, S.V.; Reich, P.B.; Frolking, S.; Lepine, L.C.; Hollinger, D.Y.; Richardson, A.D. Nitrogen cycling, forest canopy reflectance, and emergent properties of ecosystems. Proc. Natl. Acad. Sci. USA 2013, 110, E2437–E2437.
52. Ollinger, S. Sources of variability in canopy reflectance and the convergent properties of plants. New Phytol. 2011, 189, 375–394.
53. Townsend, P.A.; Serbin, S.P.; Kruger, E.L.; Gamon, J.A. Disentangling the contribution of biological and physical properties of leaves and canopies in imaging spectroscopy data. Proc. Natl. Acad. Sci. USA 2013, 110, E1074.
54. Wang, Z.; Wang, T.; Darvishzadeh, R.; Skidmore, A.K.; Jones, S.; Suarez, L.; Woodgate, W.; Heiden, U.; Heurich, M.; Hearne, J. Vegetation Indices for Mapping Canopy Foliar Nitrogen in a Mixed Temperate Forest. Remote Sens. 2016, 8, 491. https://doi.org/10.3390/rs8060491
55. Hartz, T.K. Vegetable production best management practices to minimize nutrient loss. Horttechnology 2006, 16, 398–403.
56. Thompson, R.B.; Martínez-Gaitan, C.; Gallardo, M.; Giménez, C.; Fernández, M.D. Identification of irrigation and N management practices that contribute to nitrate leaching loss from an intensive vegetable production system by use of a comprehensive survey. Agric. Water Manag. 2007, 89, 261–274, doi:10.1016/J.AGWAT.2007.01.013.
57. Thompson, R.B.; Tremblay, N.; Fink, M.; Gallardo, M.; Padilla, F.M. Tools and strategies for sustainable nitrogen fertilisation of vegetable crops. In Advances in Research on Fertilization Management in Vegetable Crops; Tei, F., Nicola, S., B nincasa, P., Eds.; Springer: Berlin/Heidelberg, Germany, 2017; pp. 11–63.
58. Congreves, K.A.; Van Eerd, L.L. Nitrogen cycling and management in intensive horticultural systems. Nutr. Cycl. Agroecosystems 2015, 102, 299–318, doi:10.1007/s10705-015-9704-7.
59. Padilla, F.M.; Gallardo, M.; Manzano-Agugliaro, F. Global trends in nitrate leaching research in the 1960–2017 period. Sci. Total Environ. 2018, 643, 400–413, doi:10.1016/j.scitotenv.2018.06.215.
60. Zotarelli, L.; Dukes, M.D.; Scholberg, J.M.S.; Muñoz-Carpena, R.; Icerman, J. Tomato nitrogen accumulation and fertilizer use efficiency on a sandy soil, as affected by nitrogen rate and irrigation scheduling. Agric. Water Manag. 2009, 96, 1247–1258, doi:10.1016/j.agwat.2009.03.019.
61. Ju, X.T.; Kou, C.L.; Zhang, F.S.; Christie, P. Nitrogen balance and groundwater nitrate contamination: Comparison among three intensive cropping systems on the North China Plain. Environ. Pollut. 2006, 143, 117–125, doi:10.1016/j.e vpol.2005.11.005.
62. Soto, F.; Gallardo, M.; Thompson, R.B.; Peña-Fleitas, M.T.; Padilla, F.M. Consideration of total available N supply reduces N fertilizer requirement and potential for nitrate leaching loss in tomato production. Agric. Ecosyst. Environ. 2015, 200, 62–70, doi:10.1016/j.agee.2014.10.022.
63. Zhu, J.H.; Li, X.L.; Christie, P.; Li, J.L. Environmental implications of low nitrogen use efficiency in excessively fertilized hot pepper (Capsicum frutescens L.) cropping systems. Agric. Ecosyst. Environ. 2005, 111, 70–80, doi:10.1016/j.agee.2005.04.025.
64. Meisinger, J.J.; Schepers, J.S.; Raun, W.R. Crop Nitrogen Requirement and Fertilization. Nitrogen Agric. Syst. 2008, 563–612, doi:10.2134/agronmonogr49.
65. Fox, R.H.; Walthall, C.L. Crop monitoring technologies to assess nitrogen status. In Nitrogen in Agricultural Systems, Agronomy Monograph No. 49; Schepers, J.S., Raun, W.R., Eds.; American Society of Agronomy, Crop Science Society of America, Soil Science Society of America: Madison, WI, USA, 2008; pp. 647–674.
66. Yao, X.; Yao, X.; Jia, W.; Tian, Y.; Ni, J.; Cao, W.; Zhu, Y. Comparison and intercalibration of vegetation indices from different sensors for monitoring above-ground plant nitrogen uptake in winter wheat. Sensors 2013, 13, 3109–3130, doi:10.3390/s130303109.

67. Mistele, B.; Schmidhalter, U. Estimating the nitrogen nutrition index using spectral canopy reflectance measurements. Eur. J. Agron. 2008, 29, 184–190.
68. Hansen, P.M.; Schjoerring, J.K. Reflectance measurement of canopy biomass and nitrogen status in wheat crops using normalized difference vegetation indices and partial least squares regression. Remote Sens. Environ. 2003, 86, 542–553, doi:10.1016/S0034-4257(03)00131-7.
69. Padilla, F.M.; Gallardo, M.; Peña-Fleitas, M.T.; de Souza, R.; Thompson, R.B. Proximal Optical Sensors for Nitrogen Ma agement of Vegetable Crops: A Review. Sensors 2018, 18, 2083, doi:10.3390/s18072083.
70. Samborski, S.M.; Tremblay, N.; Fallon, E. Strategies to make use of plant sensors-based diagnostic information for nitrogen recommendations. Agron. J. 2009, 101, 800–816.
71. Cammarano, D.; Fitzgerald, G.J.; Casa, R.; Basso, B. Assessing the robustness of vegetation indices to estimate wheat N in mediterranean environments. Remote Sens. 2014, 6, 2827–2844, doi:10.3390/rs6042827.
72. Basso, B.; Fiorentino, C.; Cammarano, D.; Schulthess, U. Variable rate nitrogen fertilizer response in wheat using remote sensing. Precis. Agric. 2015, 17, 168–182, doi:10.1007/s11119-015-9414-9.
73. Padilla, F.M.; Peña-Fleitas, M.T.; Gallardo, M.; Thompson, R.B. Determination of sufficiency values of canopy reflectance vegetation indices for maximum growth and yield of cucumber. Eur. J. Agron. 2017, 84, doi:10.1016/j.eja.2016.12.007.
74. Greenwood, D.J.; Gastal, F.; Lemaire, G.; Draycott, A.; Millard, P.; Neeteson, J.J. Growth rate and % N of field grown crops: Theory and experiments. Ann. Bot. 1991, 67, 181–190.
75. Lemaire, G.; Jeuffroy, M.H.; Gastal, F. Diagnosis tool for plant and crop N status in vegetative stage. Theory and practices for crop N management. Eur. J. Agron. 2008, 28, 614–624.
76. Lemaire, G.; Gastal, F. N Uptake and Distribution in Plant Canopies. In Diagnosis of the Nitrogen Status in Crops; Springer: Berlin/Heidelberg, Germany, 1997; pp. 3–43, ISBN 978-3-642-64506-8.
77. Hatfield, J.L.; Gitelson, A.A.; Schepers, J.S.; Walthall, C.L. Application of spectral remote sensing for agronomic decisions. Agron. J. 2008, 100, S117–S131.
78. Haboudane, D.; Miller, J.R.; Pattey, E.; Zarco-Tejada, P.J.; Strachan, I.B. Hyperspectral vegetation indices and novel algorithms for predicting green LAI of crop canopies: Modeling and validation in the context of precision agriculture. Remote Sens. Environ. 2004, 90, 337–352, doi:10.1016/j.rse.2003.12.013.
79. Fitzgerald, G.; Rodriguez, D.; O'Leary, G. Measuring and predicting canopy nitrogen nutrition in wheat using a spectral index-The canopy chlorophyll content index (CCCI). Field Crops Res. 2010, 116, 318–324, doi:10.1016/j.fcr.2010.01.010.
80. Yu, K.; Li, F.; Gnyp, M.L.; Miao, Y.; Bareth, G.; Chen, X. Remotely detecting canopy nitrogen concentration and uptake of paddy rice in the Northeast China Plain. ISPRS J. Photogramm. Remote Sens. 2013, 78, 102–115, doi:10.1016/j.isprsjprs.2013.01.008.
81. Cao, Q.; Miao, Y.; Wang, H.; Huang, S.; Cheng, S.; Khosla, R.; Jiang, R. Non-destructive estimation of rice plant nitrogen status with Crop Circle multispectral active canopy sensor. Field Crops Res. 2013, 154, 133–144, doi:10.1016/j.fcr.2013.08.005.
82. Pulido-Bosch, A.; Bensi, S.; Molina, L.; Vallejos, A.; Calaforra, J.M.; Pulido-Leboeuf, P. Nitrates as indicators of aquifer interconnection. Application to the Campo de Dalias (SE—Spain). Environ. Geol. 2000, 39, 791–799, doi:10.1007/s002540050495.
83. de Souza, R.; Peña-Fleitas, M.T.; Thompson, R.B.; Gallardo, M.; Padilla, F.M. Assessing Performance of Vegetation Indices to Estimate Nitrogen Nutrition Index in Pepper. Remote Sens. 2020, 12, 763. https://doi.org/10.3390/rs12050763
84. Muharam, F.M.; Maas, S.J.; Bronson, K.F.; Delahunty, T. Estimating Cotton Nitrogen Nutrition Status Using Leaf Greenness and Ground Cover Information. Remote Sens. 2015, 7, 7007–7028.
85. Wang, R.; Song, X.; Li, Z.; Yang, G.; Guo, W.; Tan, C.; Chen, L. Estimation of winter wheat nitrogen nutrition index using hyperspectral remote sensing. Trans. Chin. Soc. Agric. Eng. 2014, 30, 191–198.
86. Ciganda, V.S.; Gitelson, A.A.; Schepers, J. How Deep Does a Remote Sensor Sense? Expression of Chlorophyll Content in a Maize Canopy. Remote Sens. Environ. 2012, 126, 240–247.
87. Tarpley, L.; Reddy, K.R.; Sassenrath-Cole, G.F. Reflectance Indices with Precision and Accuracy in Predicting Cotton LeafNitrogen Concentration. Crop Sci. 2000, 40, 1814–1819.
88. Li, F.; Miao, Y.; Hennig, S.D.; Gnyp, M.L.; Chen, X.; Jia, L.; Bareth, G. Evaluating Hyperspectral Vegetation Indices for Estimating Nitrogen Concentration of Winter Wheat at Different Growth Stages. Precis. Agric. 2010, 11, 335–357.

89. Patel, M.K.; Ryu, D.; Western, A.W.; Suter, H.; Young, I.M. Which Multispectral Indices Robustly Measure Canopy Nitrogen across Seasons: Lessons from an Irrigated Pasture Crop. Comput. Electron. Agric. 2021, 182, 106000.
90. Wang, S.; Guan, K.; Wang, Z.; Ainsworth, E.A.; Zheng, T.; Townsend, P.A.; Li, K.; Moller, C.; Wu, G.; Jiang, C. Unique Contributions of Chlorophyll and Nitrogen to Predict Crop Photosynthetic Capacity from Leaf Spectroscopy. J. Exp. Bot. 2021, 72, 341–354.
91. Miphokasap, P.; Honda, K.; Vaiphasa, C.; Souris, M.; Nagai, M. Estimating Canopy Nitrogen Concentration in Sugarcane Using Field Imaging Spectroscopy. Remote Sens. 2012, 4, 1651–1670.
92. Hansen, P.M.; Schjoerring, J.K. Reflectance Measurement of Canopy Biomass and Nitrogen Status in Wheat Crops Using Normalized Difference Vegetation Indices and Partial Least Squares Regression. Remote Sens. Environ. 2003, 86, 542–553.
93. Ecarnot, M.; Compan, F.; Roumet, P. Assessing Leaf Nitrogen Content and Leaf Mass per Unit Area of Wheat in the Field throughout Plant Cycle with a Portable Spectrometer. Field Crops Res. 2013, 140, 44–50.
94. Li, Z.; Jin, X.; Wang, J.; Yang, G.; Nie, C.; Xu, X.; Feng, H. Estimating Winter Wheat (Triticum aestivum) LAI and Leaf Chlorophyll Content from Canopy Reflectance Data by Integrating Agronomic Prior Knowledge with the PROSAIL Model. Int. J. Remote Sens. 2015, 36, 2634–2653.
95. Yao, X.; Huang, Y.; Shang, G.; Zhou, C.; Cheng, T.; Tian, Y.; Cao, W.; Zhu, Y. Evaluation of Six Algorithms to Monitor Wheat Leaf Nitrogen Concentration. Remote Sens. 2015, 7, 14939–14966.
96. Ma, L.; Chen, X.; Zhang, Q.; Lin, J.; Yin, C.; Ma, Y.; Yao, Q.; Feng, L.; Zhang, Z.; Lv, X. Estimation of Nitrogen Content Based on the Hyperspectral Vegetation Indexes of Interannual and Multi-Temporal in Cotton. Agronomy 2022, 12, 1319. https://doi.org/10.3390/agronomy12061319
97. EO-1 (Earth Observing-1): Available online: https://www.eoportal.org/satellite-missions/eo-1#eo-1-earth-observing-1 (accessed on 22.06.2023)
98. QGIS Software: Available online: https://qgis.org/en/site/ (accessed on 24.06.2023)
99. Urfa Haber: Available online: https://www.medyaurfa.com/gundem/harran-ovasi-gap-ile-ihya-oldu-h81516.html (accessed on 26.06.2023)
100. Çimtay, Y., İlk, H. G., A novel bilinear unmixing approach for reconsideration of subpixel classification of land cover, Computers and Electronics in Agriculture, Vol. 152, pp. 126-140, 2018, https://doi.org/10.1016/j.compag.2018.07.003
101. Liwen Wang, Yaxing Wei, Revised normalized difference nitrogen index (NDNI) for estimating canopy nitrogen concentration in wetlands, Optik, Volume 127, Issue 19, 2016, Pages 7676-7688, https://doi.org/10.1016/j.ijleo.2016.05.115.
102. Rouse, J., R. Haas, J. Schell, and D. Deering. Monitoring Vegetation Systems in the Great Plains with ERTS. Third ERTS Symposium, NASA (1973): 309-317.
103. Gitelson, A., and M. Merzlyak. "Remote Sensing of Chlorophyll Concentration in Higher Plant Leaves." Advances in Space Research 22 (1998): 689-692.
104. Huete, A., et al. "Overview of the Radiometric and Biophysical Performance of the MODIS Vegetation Indices." Remote Sensing of Environment 83 (2002):195–213.
105. Sripada, R., et al. "Determining In-Season Nitrogen Requirements for Corn Using Aerial Color-Infrared Photography." Ph.D. dissertation, North Carolina State University, 2005.
106. Haboudane, D., et al. "Hyperspectral Vegetation Indices and Novel Algorithms for Predicting Green LAI of Crop Canopies: Modeling and Validation in the Context of Precision Agriculture." Remote Sensing of Environment 90 (2004): 337-352.
107. Vogelmann, J., B. Rock, and D. Moss. "Red Edge Spectral Measurements from Sugar Maple Leaves." International Journal of Remote Sensing 14 (1993): 1563-1575.
108. Serrano, L., J. Penuelas, and S. Ustin. "Remote Sensing of Nitrogen and Lignin in Mediterranean Vegetation from AVIRIS Data: Decomposing Biochemical from Structural Signals." Remote Sensing of Environment 81 (2002):355-364.
109. Deep Learning Toolbox. Available online: https://www.mathworks.com/products/deep-learning.html (accessed on 28.06.2023).

 doi:10.20944/preprints202307.1328.v1

110. Hagan, M. T., and Menhaj, M. B. "Training feedforward networks with the Marquardt algorithm." IEEE transactions on Neural Networks 5, no. 6 (1994): 989-993.
111. Wang, F-Y. "Control 5.0: from Newton to Merton in popper's cybersocial-physical spaces." IEEE/CAA Journal of Automatica Sinica 3, no. 3, (2016): 233-234.